Engineering Failure Analysis 84 (2018) 247–261

Contents lists available at ScienceDirect

Engineering Failure Analysis

journal homepage: www.elsevier.com/locate/engfailanal

Failure of the bucket wheel excavator buckets

Srđan M. Bošnjak[a,*], Miodrag A. Arsić[b], Nebojša B. Gnjatović[a], Ivan L.J. Milenović[a], Dušan M. Arsić[c]

[a] University of Belgrade, Faculty of Mechanical Engineering, Kraljice Marije 16, 11120, Belgrade 35, Serbia
[b] Institute for Testing of Materials IMS, Bulevar Vojvode Mišića 43, 11000 Belgrade, Serbia
[c] University of Kragujevac, Faculty of Engineering, Sestre Janjić 6, 34000 Kragujevac, Serbia

ARTICLE INFO

Keywords:
Bucket wheel excavator
Bucket
Failure
Experimental investigation
Linear finite element analysis

ABSTRACT

Buckets are a vital substructure of all digging machines, and are intended for the realisation of the fundamental machine function - soil excavation. This paper presents the results of the experimental-numerical investigation of the cause of the bucket wheel excavator SRs 470 buckets failure. The chemical composition and mechanical properties, the impact toughness, hardness, tendency to cracks and the microstructure were determined using appropriate tests. Experimental examinations of working and residual stresses were performed using strain gauges. The superposition of the experimentally determined working and residual stresses and the calculation of the total principal stresses were conducted using the originally developed procedure presented in this paper. The bucket working stress state was calculated by applying the linear finite element method. Conclusions based on the investigation results show that the main reasons for the buckets failure were the 'design-in defects' - oversights made during the procedures of geometrical shaping and material selection. Furthermore, high values of residual stresses, as well as the cold cracking observed on the welded joint of the knife and the bucket body, suggest that the 'manufacturing-in defects' also played a significant role in the failure. The superposition of influences of the 'design-in defects' and the 'manufacturing-in defects' has conditioned the appearance and propagation of long-term fatigue cracks, leading to the total destruction of the buckets. The fact that buckets' failure appeared due to oversights made during geometrical shaping, material selection and manufacturing further points to the importance of the critical approach implementation during the design phase of the earthmoving machines working devices.

1. Introduction

The exploitation of bucket wheel excavators (BWE) in harsh working conditions, accompanied by loads of pronounced dynamic and stochastic character, leads to failures of their structural as well as mechanism parts [1–5].

This paper analyses the case of structural failures [6] of the BWE SRs 470 buckets, which occurred during coal excavation, Fig. 1. The coal block was relatively homogeneous, with rare and thin layers of hard sand/rock. According to the measurements conducted 'in situ', the obtained value of the cutting resistance per unit of cutting edge length was $k_{L,c} = 84$ kN/m for coal and $k_{L,hl} = 98$ kN/m for hard sand/rock layers, while the specific cutting force achievable by the excavating device had the value of 107 kN/m. The excavation was realised using the combined method with a dominant participation of the terrace cutting. The drop cutting method was used for the excavation of hard layers. It was obvious, Fig. 1, that the level of the buckets' degradation was so pronounced that

* Corresponding author.
E-mail address: sbosnjak@mas.bg.ac.rs (S.M. Bošnjak).

https://doi.org/10.1016/j.engfailanal.2017.11.017
Received 12 September 2017; Received in revised form 24 November 2017; Accepted 28 November 2017
Available online 29 November 2017
1350-6307/ © 2017 Elsevier Ltd. All rights reserved.

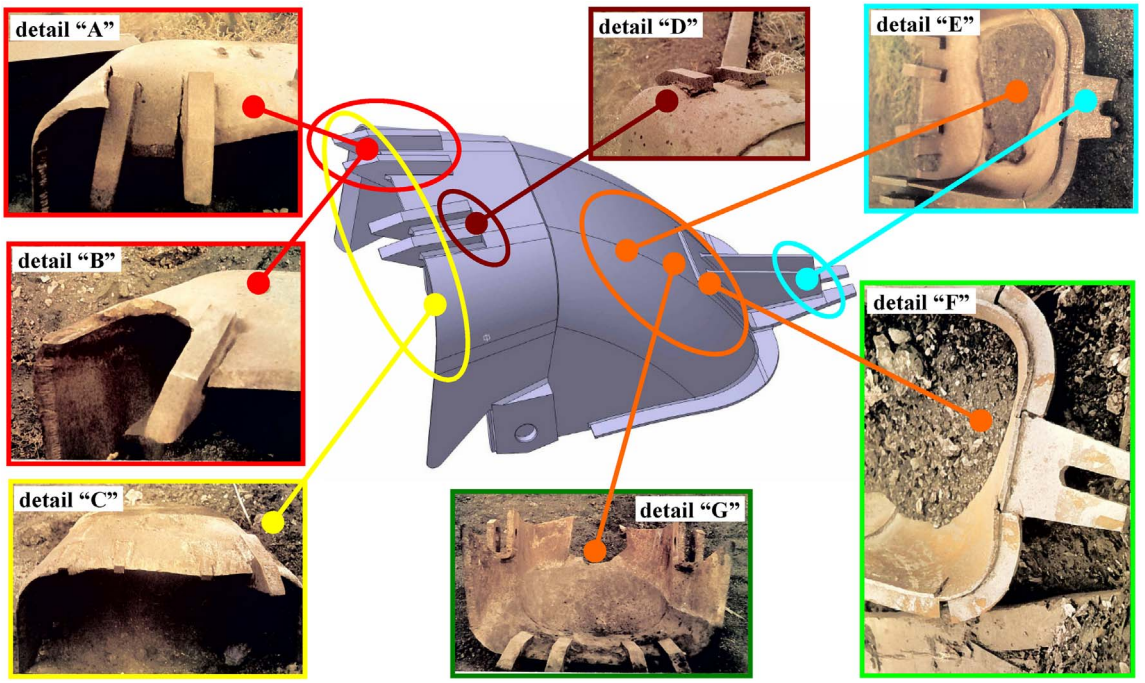

Fig. 1. Damage to the buckets' structure: details A, B, C, D – damage of the teeth and knife; details E, F, G – damage to the buckets' back and zones of rear wedge fastening.

they were practically unusable, leading to the conclusion that their repairing would be entirely unreasonable. In order to diagnose the cause of the bucket body damages, the following steps had to be performed:

- An experimental procedure which included: chemical composition and mechanical properties of base metal (BM); impact toughness and hardness; tendency to cracks; microstructure examinations; working and residual stress analyses using strain gauges, and
- The calculation of the bucket working stress state applying the linear finite element method (LFEM).

The presented investigation results are important for the following reasons:

- Buckets present the vital substructure of all digging machines, intended for the realisation of the fundamental machine function (soil excavation). Their structural failure leads to the appearance of direct and indirect losses caused by the complete system standstill [6];
- Specialized literature on the subject of BWE and working devices of earthmoving machines [7–13] does not deal with the problems of geometrical shaping and strength of buckets adequately, considering the importance of the mentioned substructures.

2. Experimental procedure

According to the design documentation, the bucket body was supposed to be made from steel quality grade S235J2G3 [14], while the bucket knife as well as the eye-plates of the front supports were supposed to be made from steel quality grade E335 [14].

2.1. Chemical composition, tensile properties, impact toughness, hardness and tendency to cracks

Chemical analyses of the bucket body (samples taken from two series of buckets) (Table 1) and the bucket knife material (Table 2)

Table 1
Chemical analysis (wt%) of the bucket body material and chemical composition of S235J2G3 [14].

Material	C	Si	P	S	Mn
Batch 1	0.080	0.215	0.012	0.033	0.390
Batch 2	0.155	0.230	0.028	0.025	0.460
S235J2G3	Max. 0.19	–	Max. 0.035	Max. 0.035	Max. 1.50

Table 2
Chemical analysis (wt%) of the bucket knife material and chemical composition of E335 [14].

Material	C	Si	P	S	Mn
Batch 1	0.320	0.340	0.023	0.029	1.290
Batch 2	0.250	0.275	0.033	0.015	1.620
E335	–	–	Max. 0.055	Max. 0.055	–

were conducted by the spectrometric method using the quantometer ARL 360.

Tensile tests (Tables 3 and 4) were carried out in a universal A.J. Amsler testing machine, according to the requirements of the code [15].

Determination of the Charpy impact toughness of welded joints was conducted on standard test specimens [16,17], sampled from the buckets that were used in exploitation (Tables 5 and 6).

Average values, obtained for five measurements of bucket body and knife material macrohardness, were equal to 121 HB and 169 HB [18], respectively.

Hot cracks were not detected by the FISCO test [19] on the two specimens sampled from the bucket body nor on the two specimens sampled from the bucket knife. The existence of cold cracks was also not detected by the CTS tests on the two specimens sampled from the bucket body. However, on one specimen, sampled from the bucket knife, a cold crack was observed (Fig. 2).

2.2. Microstructure examinations

Microstructure testing [20] is based on the replicas [21] taken from the welded joints of the bucket body (Figs. 3–5).

2.3. Experimental stress identification

2.3.1. Strain measurement

For measurement of the strains during excavation, i.e. working strains, besides the right-angled (0°/45°/90°) rosettes HBM RY11 (measuring points – MPs – 3,4,6,7,9 and 10), right-angled (0°/45°/90°) rosettes HBM RY61 (MPs 1,2,5,8,11,12 and 13) were used as well (Fig. 6, Table 7). They were also used for the relaxation strains measurements (Table 8) which were carried out by the centre hole drilling method (Fig. 7). The relaxation strains measurements at measuring points MP1, MP2, MP5 and MP8 had been conducted prior to the measurement of working strains, while the measurement at measuring points MP11, MP12 and MP13 was carried out after. During the working strains diagnostics, a failure of rosettes appeared in measuring points MP2, MP3 and MP10. The measurements were conducted when ≈ 75% of the nominal bucket wheel drive power was engaged.

2.3.2. Calculation of working and residual stresses

The principal stress values (σ_1 and σ_2) (Tables 9 and 10) were determined on the basis of the strain values measured during excavation (superscript "*w*") [22]

$$\sigma_{1,2}^{w} = \frac{E}{1-\nu}\frac{\varepsilon_a^w + \varepsilon_c^w}{2} \pm \frac{E}{\sqrt{2}(1+\nu)}\sqrt{(\varepsilon_a^w - \varepsilon_b^w)^2 + (\varepsilon_c^w - \varepsilon_b^w)^2}, \tag{1}$$

and on the basis of the relaxation strain values (superscript "*r*") [22]

$$\sigma_{1,2}^{r} = -\frac{E}{4A}(\varepsilon_a^r + \varepsilon_c^r) \pm \frac{E}{4B}\sqrt{(\varepsilon_c^r - \varepsilon_a^r)^2 + (\varepsilon_a^r + \varepsilon_c^r - 2\varepsilon_b^r)^2}, \tag{2}$$

where $E = 210{,}000$ MPa and $\nu = 0.3$ are Young's modulus and Poisson's ratio of the bucket material, while ε_a, ε_b and ε_c are the measured values of strains in referent directions (a: 0; b: 45°; c: 90°). For the rosette HBM RY61, the values of constants A and B, Eq. (2), are were determined according to the expressions [22]

Table 3
Tension tests [15] results of the bucket body material and tensile properties of S235J2G3 [14].

Material	Specimen	σ_{YS}	Average	σ_{UTS}	Average	Elongation A5	Average
		MPa				%	
Batch 2	1	271.3		405.2		21.3	
	2	275.4		420.7		26.9	
	3	285.6	279.6	435.4	424.6	24.4	23.6
	4	280.8		430.7		22.5	
	5	285.0		431.2		23.1	
S235J2G3		Min. 235		340–510		Min. 26	

Table 4
Tension tests [15] results of the bucket knife material and tensile properties of E335 [14].

Material	Specimen	σ_{YS}	Average	σ_{UTS}	Average	Elongation A5	Average
		MPa				%	
Batch 2	1	348.9	347.2	599.3	598.9	31.7	33.8
	2	345.4		598.4		35.8	
E335		Min. 325		570–710		Min. 16	

Table 5
Impact toughness of test specimen with V-shaped notch in the weld face.

Specimen	Temperature (°C)	Impact toughness (J/cm^2)	Average (J/cm^2)
1	− 20	88.1	
2	− 20	42.6	60.7
3	− 20	51.5	
4	0	56.4	
5	0	59.4	59.5
6	0	62.7	
7	20	107.8	
8	20	121.8	120
9	20	130.4	

Table 6
Impact toughness of test specimen with V-shaped notch in the weld root.

Specimen	Temperature (°C)	Impact toughness (J/cm^2)	Average (J/cm^2)
1	− 20	59.4	
2	− 20	62.7	58.2
3	− 20	52.4	
4	0	98.0	
5	0	85.2	84.5
6	0	70.3	
7	20	102.9	
8	20	93.1	95.0
9	20	89.1	

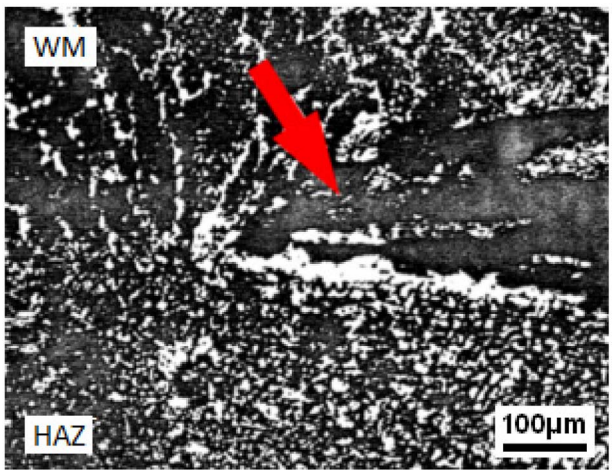

Fig. 2. Bucket knife: transition zone weld metal (WM)-heat affected zone (HAZ) with cold crack along the weld line (etched with 3% nital).

$$A = 0.04735(1 + \nu), \tag{3}$$

$$B = 0.1894 - 0.01515(1 + \nu). \tag{4}$$

Equivalent stress values (Tables 9 and 10) were calculated using the von Misses hypothesis,

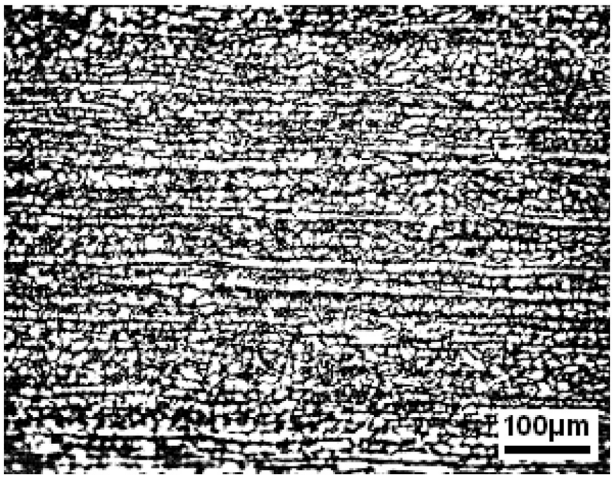

Fig. 3. Lamellar ferrite/pearlite microstructure of BM (etched with 3% nital).

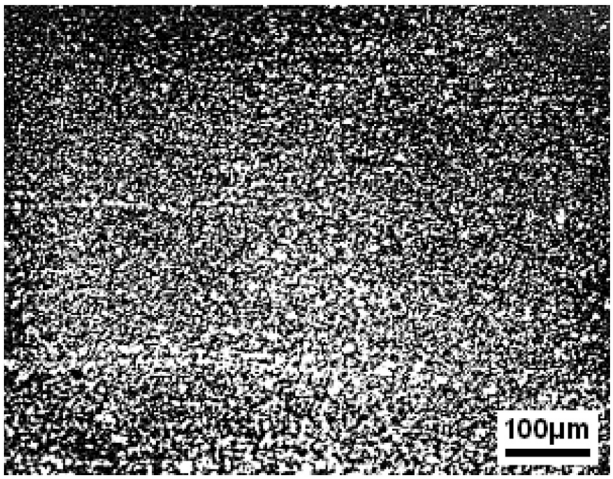

Fig. 4. Fine grain ferrite/pearlite microstructure of HAZ (etched with 3% nital).

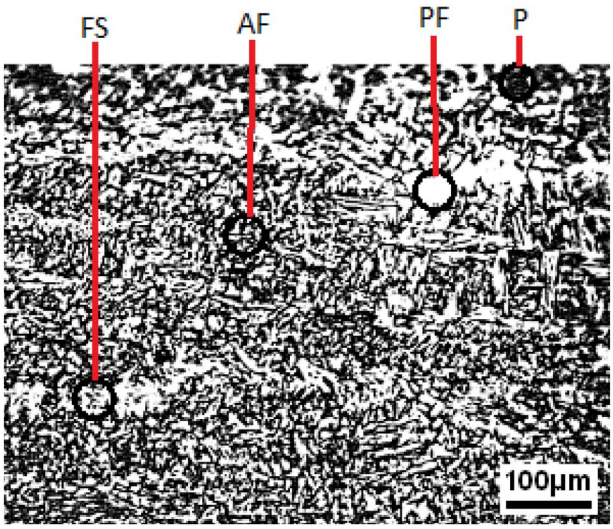

Fig. 5. WM zone microstructure: acicular ferrite (AF), ferrite with second phase (FS), polygonal ferrite (PF) and pearlite (P), with local presence of small non-metallic inclusions (etched with 3% nital).

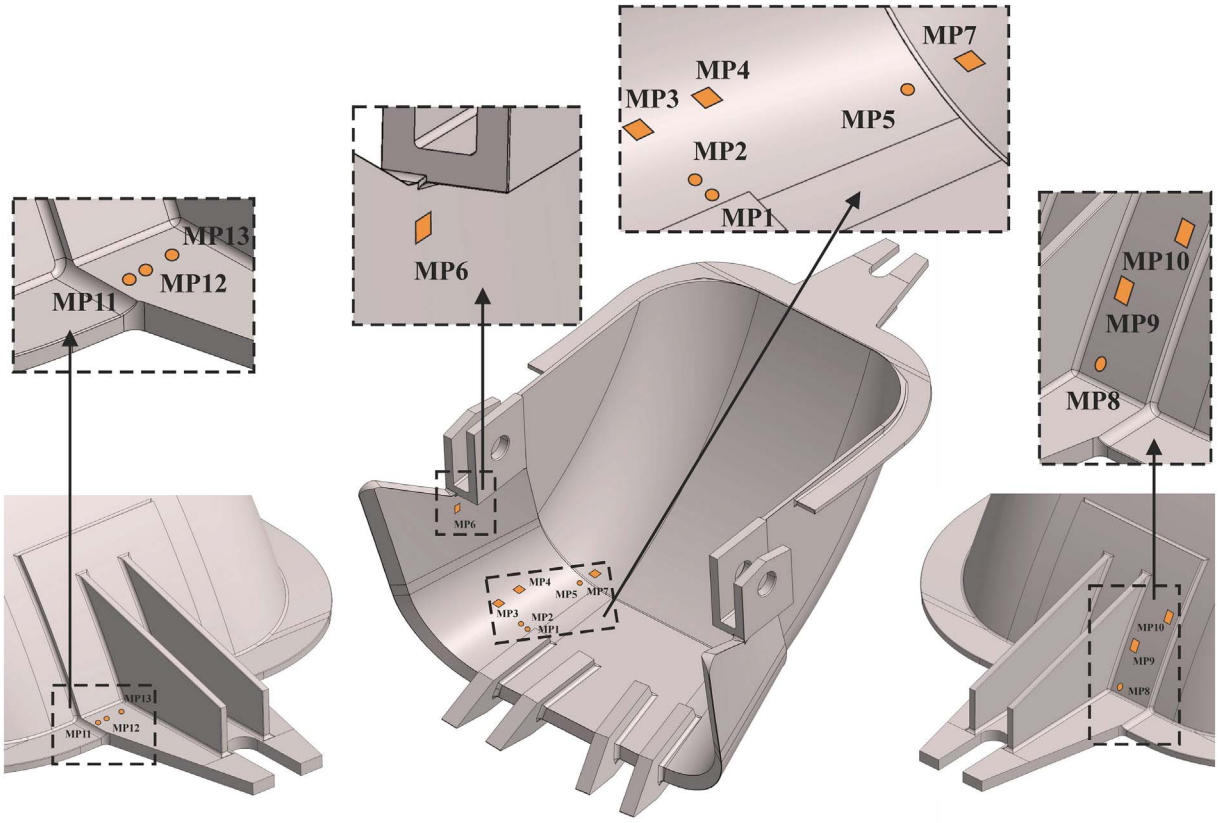

Fig. 6. Locations of measuring points ("squares": RY11; "circles": RY61).

Table 7
Reference values of working strains.

Measuring point	$\varepsilon_a{}^w \times 10^6$	$\varepsilon_b{}^w \times 10^6$	$\varepsilon_c{}^w \times 10^6$
1	833.3	615.4	− 774.2
4	− 461.5	− 595.7	− 615.4
5	− 333.3	− 307.7	− 363.6
6	224.0	− 232.7	232.3
7	276.9	− 300.0	288.0
8	288.0	− 400.0	− 384.0
9	− 384.6	322.6	− 241.9

Table 8
Reference values of relaxation strains.

Measuring point	$\varepsilon_a{}^r \times 10^6$	$\varepsilon_b{}^r \times 10^6$	$\varepsilon_c{}^r \times 10^6$
1 (HAZ)	− 115.0	81.2	58.8
2 (BM)	13.5	− 135.0	14.0
5 (HAZ)	57.0	− 66.0	19.5
8 (HAZ)	122.4	91.8	− 71.4
11 (WM)	− 97.2	− 86.4	− 41.9
12 (HAZ)	− 81.9	− 90.3	− 31.5
13 (BM)	− 51.3	− 91.2	− 39.9

$$\sigma_{eq} = \sqrt{\sigma_1^2 + \sigma_2^2 - \sigma_1\sigma_2}. \tag{5}$$

2.3.3. *Superposition of working and residual stresses*

By implementing the reduced modulus of elasticity,

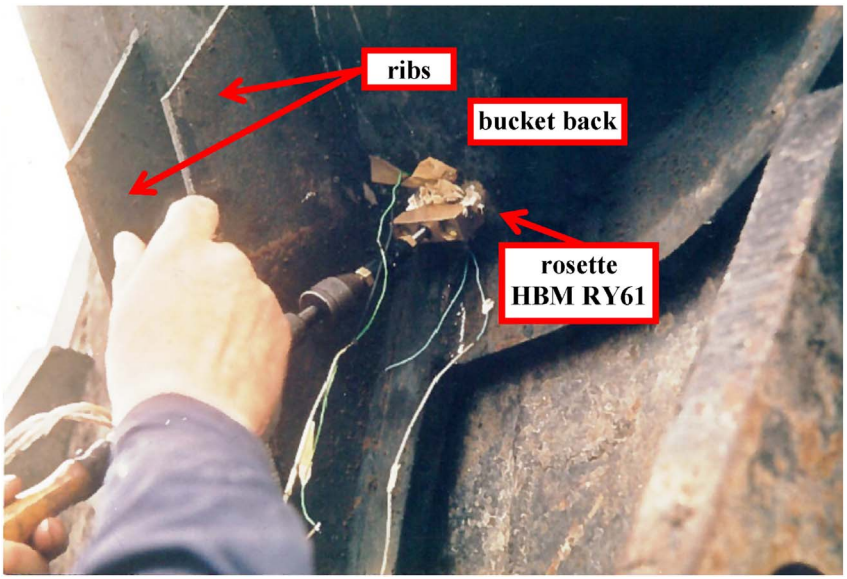

Fig. 7. Measurement of residual stresses in the zone of rear fastening.

Table 9
Principal and equivalent working stresses.

Measuring point	σ_1^w (MPa)	σ_2^w (MPa)	σ_{eq}^w (MPa)
1	169.5	− 151.8	278.4
4	− 146.1	− 177.0	163.8
5	− 97.5	− 111.6	105.3
6	142.9	− 6.0	146.0
7	178.8	− 9.4	183.7
8	64.2	− 93.0	136.9
9	9.4	− 197.3	202.2

Table 10
Principal and equivalent residual stresses.

Measuring point	σ_1^r (MPa)	σ_2^r (MPa)	σ_{eq}^r (MPa)
1 (HAZ)	134.4	− 38.5	157.2
2 (BM)	68.6	− 115.4	161.1
5 (HAZ)	0.3	− 130.8	130.9
8 (HAZ)	29.2	− 116.1	133.1
11 (WM)	138.7	98.5	123.6
12 (HAZ)	122.7	70.7	106.7
13 (BM)	106.2	49.3	92.1

$$E_1 = \frac{E}{1-\nu}, \tag{6}$$

$$E_2 = \frac{E}{1+\nu}, \tag{7}$$

$$E_3 = -\frac{1}{2}\frac{E}{A} = -\frac{1}{2}\frac{E}{0.04735(1+\nu)} = -\frac{E}{0.0947(1+\nu)}, \tag{8}$$

$$E_4 = \frac{1}{2}\frac{E}{B} = \frac{1}{2}\frac{E}{0.1894 - 0.01515(1+\nu)} = \frac{E}{0.3788 - 0.0303(1+\nu)}, \tag{9}$$

expressions (1) and (2) yield to the form

Table 11
Total principal and equivalent stresses.

Measuring point	σ_1^{tot} (MPa)	σ_2^{tot} (MPa)	σ_{eq}^{tot} (MPa)
1 (HAZ)	236.1	− 122.4	315.6
5 (HAZ)	− 110.2	− 229.4	198.7
8 (HAZ)	57.4	− 173.2	208.0

$$\sigma_{1,2}^{w} = \frac{1}{2}E_1(\varepsilon_a^{w} + \varepsilon_c^{w}) \pm \frac{E_2}{\sqrt{2}}\sqrt{(\varepsilon_a^{w} - \varepsilon_b^{w})^2 + (\varepsilon_c^{w} - \varepsilon_b^{w})^2} =$$
$$= \frac{1}{2}E_1(\varepsilon_a^{w} + \varepsilon_c^{w}) \pm \frac{1}{2}E_2\sqrt{2[(\varepsilon_a^{w} - \varepsilon_b^{w})^2 + (\varepsilon_c^{w} - \varepsilon_b^{w})^2]} =$$
$$= \frac{1}{2}E_1(\varepsilon_a^{w} + \varepsilon_c^{w}) \pm \frac{1}{2}E_2\sqrt{(\varepsilon_a^{w} - \varepsilon_c^{w})^2 + (2\varepsilon_b^{w} - \varepsilon_a^{w} - \varepsilon_c^{w})^2}, \tag{10}$$

$$\sigma_{1,2}^{r} = \frac{1}{2}E_3(\varepsilon_a^{r} + \varepsilon_c^{r}) \pm \frac{1}{2}E_4\sqrt{(\varepsilon_c^{r} - \varepsilon_a^{r})^2 + (\varepsilon_a^{r} + \varepsilon_c^{r} - 2\varepsilon_b^{r})^2} =$$
$$= \frac{1}{2}E_3(\varepsilon_a^{r} + \varepsilon_c^{r}) \pm \frac{1}{2}E_4\sqrt{(\varepsilon_a^{r} - \varepsilon_c^{r})^2 + (2\varepsilon_b^{r} - \varepsilon_a^{r} - \varepsilon_c^{r})^2}. \tag{11}$$

Having in mind the fact that the expressions (10) and (11) are of an analogue form, it is possible to conduct the superposition of influences of working and relaxation strains and to determine total principal stresses,

$$\sigma_{1,2}^{tot} = \frac{1}{2}[E_1(\varepsilon_a^{w} + \varepsilon_c^{w}) + E_3(\varepsilon_a^{r} + \varepsilon_c^{r})] \pm$$
$$\pm \frac{1}{2}\sqrt{[E_2(\varepsilon_a^{w} - \varepsilon_c^{w}) + E_4(\varepsilon_c^{r} - \varepsilon_a^{r})]^2 + [E_2(2\varepsilon_b^{w} - \varepsilon_a^{w} - \varepsilon_c^{w}) + E_4(\varepsilon_a^{r} + \varepsilon_c^{r} - 2\varepsilon_b^{r})]^2}. \tag{12}$$

Afterwards, the total equivalent stress is calculated according to Eq. (5) (Table 11).

An alternative approach to the working and residual stresses superposition is also feasible. Namely, after determining the principal residual stresses in the observed measuring point (Table 9) it is possible to calculate the working stresses in regard to the principal directions of residual stresses or vice versa. During the procedure, besides the normal ones, the corresponding shear stresses would appear as well. After determining the stress state in this manner, the total equivalent stress is calculated. This procedure requires, among other things, the determination of the principal directions of the working and residual stresses; it is longer than the procedure of determining total principal stresses according to the expression (12) and, at the same time, gives, naturally, the same results. For these reasons, the procedure of determining total principal stresses according to the expression (12) has been presented and used.

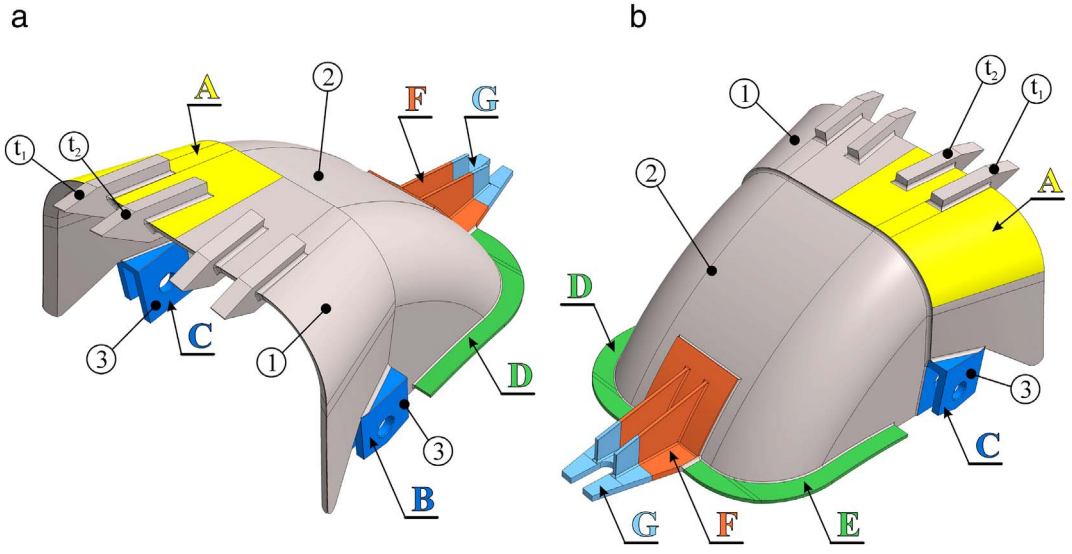

Fig. 8. 3D model of the bucket (1-bucket knife; 2-bucket back; 3-end eyes of the front supports; A–G: critical zones; t_1, t_2: designation of the tooth position): (a) front view; (b) rear view.

Table 12
Equivalent (von Misses) stress values (MPa) in bucket critical zones.

LC	Critical zone (see Fig. 8)						
	A	B	C	D	E	F	G
1 (1/1/1/1)	321.8	129.2	122.1	203.2	88.5	406.5	531.9
2 (1/1/1/2)	271.8	165.0	148.1	150.2	196.0	373.8	562.2
3 (1/1/2/1)	301.5	138.5	212.1	228.2	58.1	419.7	589.9
4 (1/1/2/2)	275.3	242.7	127.3	152.1	175.7	384.5	618.2
5 (1/2/1/1)	789.7	191.4	215.7	250.0	64.6	422.8	567.2
6 (1/2/1/2)	667.6	323.4	144.8	163.6	179.3	385.3	595.3
7 (1/2/2/1)	626.5	275.4	264.8	259.5	59.8	431.1	642.3
8 (1/2/2/2)	550.5	408.1	144.6	163.6	182.1	395.1	670.4
9 (2/1/1/1)	415.4	150.5	156.4	255.0	115.3	522.4	691.3
10 (2/1/1/2)	350.8	202.1	112.3	192.9	171.7	480.5	721.2
11 (2/1/2/1)	379.3	182.0	262.1	253.3	74.0	528.3	753.0
12 (2/1/2/2)	349.8	302.9	150.5	194.8	177.8	493.0	781.4
13 (2/2/1/1)	1013.0	262.4	266.7	284.3	83.4	530.0	723.4
14 (2/2/1/2)	891.03	407.8	145.2	210.3	180.0	494.0	751.5
15 (2/2/2/1)	804.4	372.1	330.5	294.3	75.9	542.9	820.8
16 (2/2/2/2)	726.1	518.8	185.6	210.2	185.2	506.7	849.1

3. Numerical identification of the bucket stress states

Identification of the bucket stress states was performed by applying the LFEM. The 3D model of the bucket (Fig. 8) represents the continuum discretised by the 4-node linear tetrahedron elements in order to create the FEM model (619,023 nodes and 379,511 elements). The bucket loading, caused by the resistance to excavation, was determined according to the procedures presented in [2,7–10,13].

The LFEM analyses (Table 12) were done for the set of load cases (LCs) determined by the designation *a/b/c/d*, where:

a - the identifier of the intensity of the tangential component of force resisting excavation (Fig. 9a): $a = 1$ if the tangential component is calculated based on the nominal BW drive parameters ($W_{t,nom} = 132$ kN); $a = 2$ if the mentioned component is calculated based on the limit BW drive parameters ($W_{t,max} = 172$ kN);
b - the identifier of the set of coefficients k_r and k_l on the basis of which the intensities of radial ($W_r = k_r W_t$) and lateral ($W_l = k_l W_t$) components of force resisting excavation are determined (Fig. 9a); according to the [8–10], the bucket load analysis is performed for two groups of values of k_r and k_l: $k_r = 0.5$, $k_l = 0.35$ ($b = 1$) and $k_r = 0.8$, $k_l = 0.5$ ($b = 2$);
c – the identifier of the tooth exposed to the force resisting excavation [2,13]; $c = 1$ when the mentioned load affects tooth t_1 and $c = 2$ when the load acts on tooth t_2 (Fig. 8);
d - the identifier of the bucket constraints: $d = 1$ for the case shown in Fig. 9a; $d = 2$ for the case shown in Fig. 9b.

Having in mind the number of possible values of the previously mentioned identifiers ($n_a = n_b = n_c = n_d = 2$), it is conclusive that the total LCs number is $n_{LC} = 2^4 = 16$.

The buckets stress fields obtained for the action of loads, calculated for the limit bucket wheel drive parameters, are presented in Fig. 10. Maximum values of equivalent stress in critical zones (Fig. 8), for all of the analysed LCs, are presented in Table 12.

4. Discussion

The analyses of data presented in Tables 1–4 lead to the conclusion that both the chemical composition and the tensile properties of the bucket body and knife materials meet the requirements of the standard [14]. Furthermore, satisfactory toughness of the bucket body material welded joints is obtained (Tables 5 and 6).

The base material has a lamellar ferrite/pearlite microstructure which is the consequence of rolling (Fig. 3). The fine grained ferrite/pearlite microstructure of HAZ (Fig. 4) is obtained by fast cooling and is characterised by higher toughness. The microstructure of the weld metal (Fig. 5) is common for the welded joints of structural steels: acicular ferrite, ferrite with second phase, polygonal ferrite and pearlite, with the local presence of small non-metallic inclusions.

In testing conditions – engagement of ≈ 75% of nominal bucket wheel drive power – the maximum experimentally determined working stress value on the knife of the bucket ($\sigma_{eq}{}^{w} = 278.4$ MPa, MP1, Table 9) is 19% lower than the experimentally determined minimum yield stress value ($\sigma_{YS,\,min}{}^{k} = 345.4$ MPa, Table 4, Fig. 11a). For the bucket body, the maximum experimentally determined working stress value ($\sigma_{eq}{}^{w} = 202.2$ MPa, MP9, Table 9) is 25.5% lower than the experimentally determined minimum yield stress value ($\sigma_{YS,\,min}{}^{b} = 271.3$ MPa, Table 3, Fig. 12a).

The values of residual stresses are extremely high (Table 10). These values reach 46.6% of the minimum experimentally determined yield stress value for the knife (MP2) and 49.1% for the bucket body (MP8), which is, according to [23], almost on the verge of acceptability of the results obtained by the centre hole drilling method.

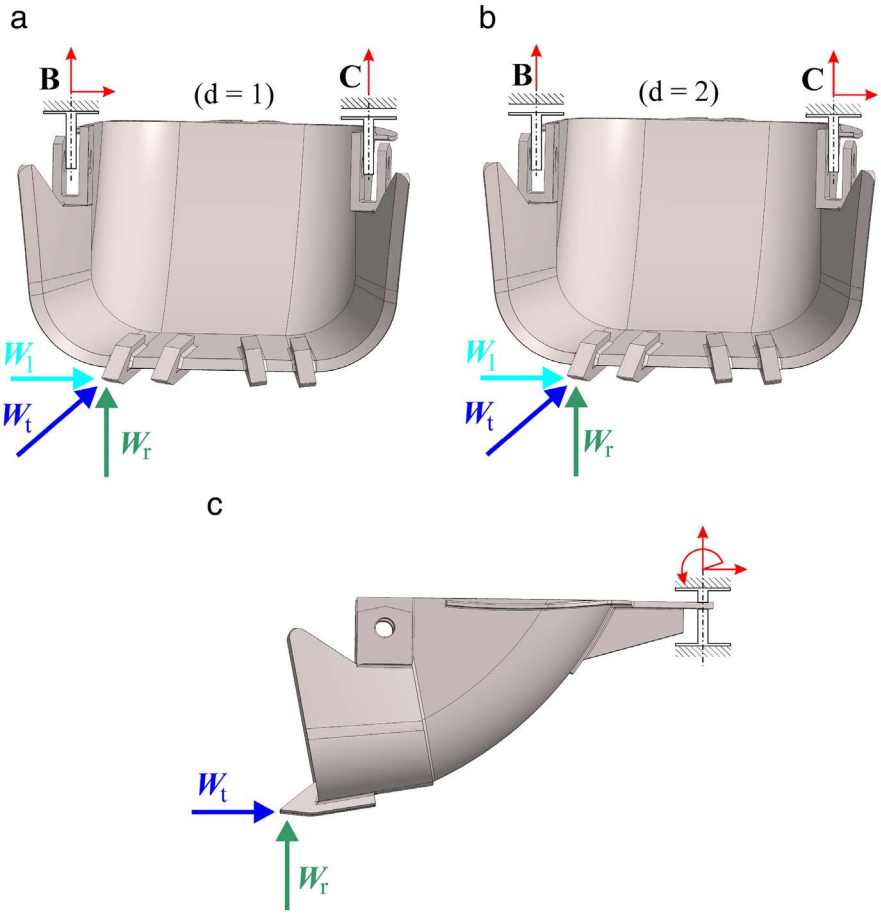

Fig. 9. Bucket constraints and loads: (a) lateral abutment of front/right fastening ($d = 1$); (b) lateral abutment of front/left fastening ($d = 2$); (c) rear side fastening.

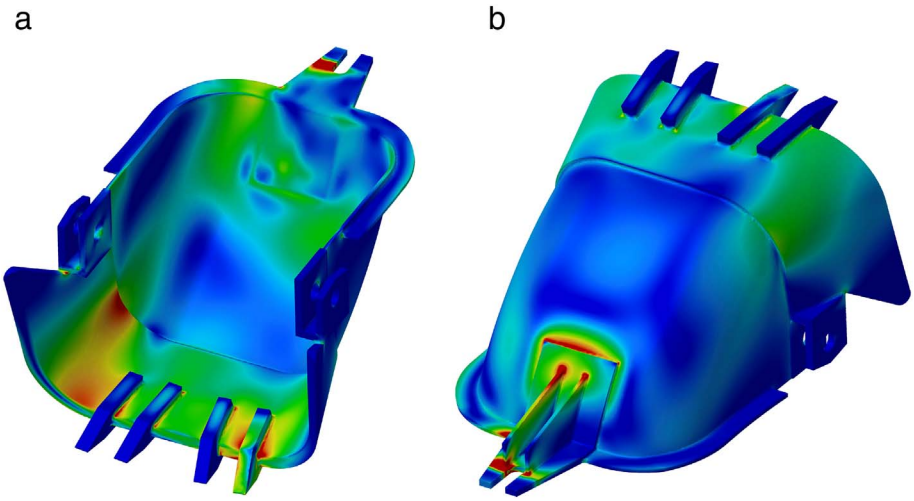

Fig. 10. Von Misses stress fields (in red coloured areas stress values are higher than 355 MPa): (a) LC 2/2/1/2 (compare with details A–D in Fig. 1); (b) LC 2/1/2/1 (compare with details E–G in Fig. 1). (For interpretation of the references to colour in this figure legend, the reader is referred to the web version of this article.)

By superpositioning the experimentally obtained working and residual stresses (Table 11) it is determined that the equivalent stress values reach 91.4% of the minimum experimentally determined yield stress value for the knife ($\sigma_{eq}{}^{tot} = 315.6$ MPa, MP1) and 76.7% of the bucket body minimum experimentally determined yield stress value ($\sigma_{eq}{}^{tot} = 208.0$ MPa, MP8). The values of equivalent stresses are extremely high, especially having in mind the fact that the measurements of working stresses were conducted

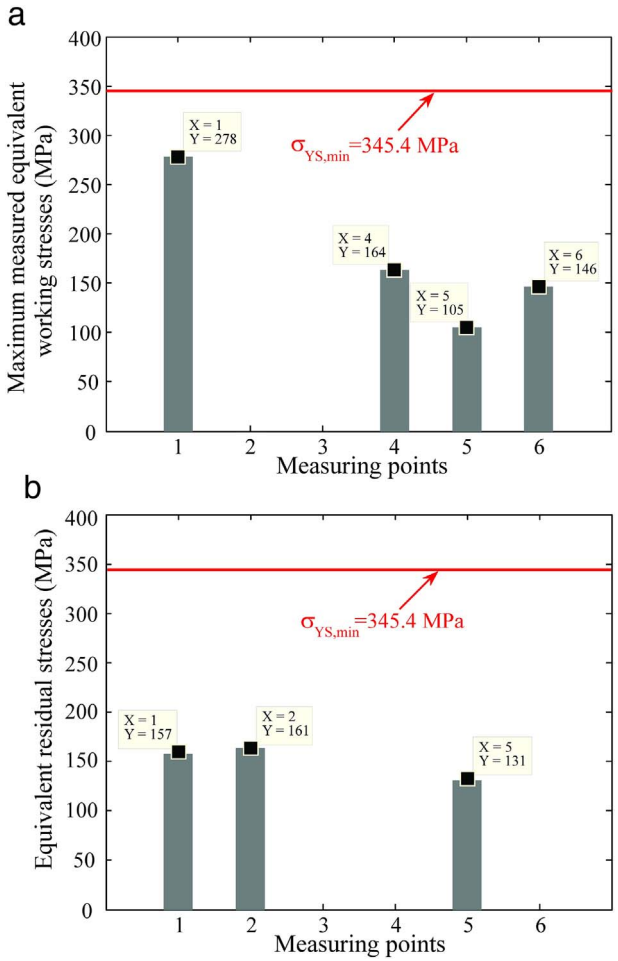

Fig. 11. Equivalent stress values of the bucket knife determined by measurements: (a) maximum working stresses; (b) residual stresses.

when ≈ 75% of nominal bucket wheel drive power was engaged.

The ratio between the equivalent working stress determined by measurement (Table 9) (bucket knife: $\sigma_{eq,\ MP1}{}^{w} > \sigma_{eq,\ MP4}{}^{w} > \sigma_{eq,\ MP6}{}^{w} > \sigma_{eq,\ MP5}{}^{w}$; bucket body: $\sigma_{eq,\ MP9}{}^{w} > \sigma_{eq,\ MP7}{}^{w} > \sigma_{eq,\ MP8}{}^{w}$), is in full compliance with the ratio of the maximum calculated values of equivalent working stresses (Fig. 10). It is not possible to compare the exact numerical values of equivalent stresses determined by measurement and the LFEM, since neither the investigation of load distribution across buckets (which are in interaction with the soil) nor the distribution of loads across teeth was taken into account during the experiment.

Having in mind that stress calculation was performed using the LFEM, the obtained equivalent stress values higher than the proportionality limits of the bucket knife as well as the bucket body materials should be analysed only as indicators of inadmissible high stress states, and not as the exact stress values (Figs. 13 and 14).

For the nominal intensity of the tangential component of the resistance to excavation ($a = 1$) and lower values of the coefficients k_r and k_l ($b = 1$), stress values of the bucket knife (zone A) are lower than the minimum yield stress value, LCs 1–4 (Fig. 13, Table 12). When higher values of the coefficients k_r and k_l are considered ($b = 2$), for the LCs 5–7, stress values obtained for the bucket knife are higher than the ultimate strength, while for the LC 8 the analysed values are considerably higher than the yield stress value (Fig. 13, Table 12). For maximum intensity of the tangential component of the resistance to excavation ($a = 2$) and lower values of the coefficients k_r and k_l ($b = 1$), stress values obtained for the bucket knife are higher than the minimum yield stress value, LCs 9–12 (Fig. 14, Table 12) while when $b = 2$ the mentioned values are higher than the ultimate strength, LCs 13–16.

In front bucket supports (zones B and C), which are produced of the same material as the bucket knife, under the nominal intensity of the tangential component of the resistance to excavation ($a = 1$), the obtained stress values are lower than the yield stress value, except for the LC 8 (Fig. 13, Table 12). Under the maximum intensity of the tangential component of resistance to excavation ($a = 2$), the stress values are also lower than the yield stress value for LCs 9–13, while being higher for all of the other analysed LCs (Fig. 14, Table 12).

In zones D and E, the calculated stress values are lower than the yield stress value for all load cases (Figs. 13 and 14, Table 12) except for the LC 13 and LC 15, for which they are slightly higher.

In all of the considered load cases, the values of stresses in the bucket back (zones F and G) are very high. In zone F, the calculated

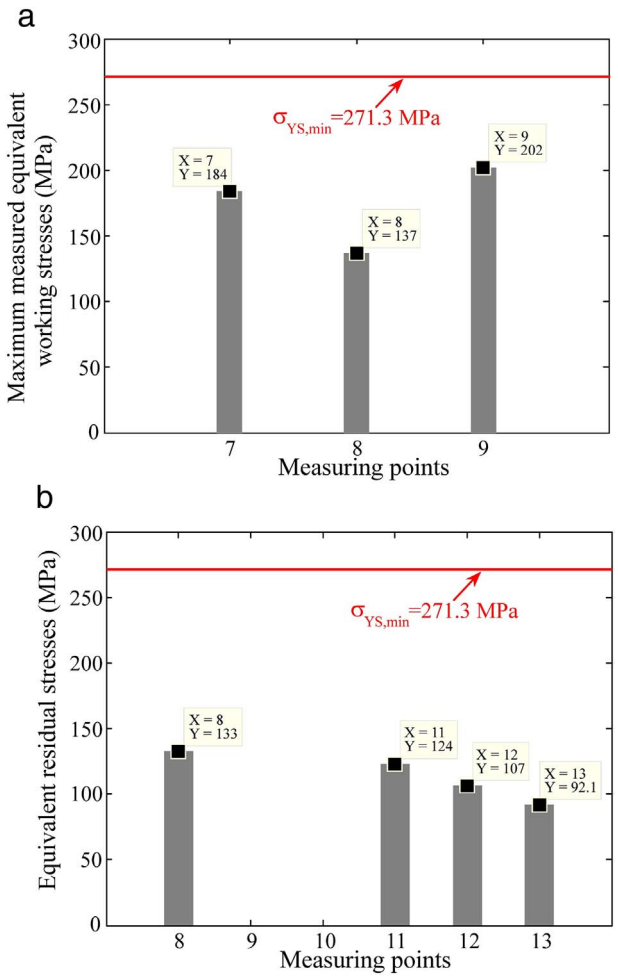

Fig. 12. Equivalent stress values of the bucket body determined by measurements: (a) maximum working stresses; (b) residual stresses.

stress values are below the minimum ultimate strength only in LCs 2, 4, 6 and 8, while the obtained values in zone G are higher than the minimum ultimate strength value in all considered load cases (Figs. 13 and 14, Table 12).

Based on the analysis of the calculated working stresses presented above, it is conclusive that the bucket knife and the bucket back are critical subdomains of the bucket structure, which is confirmed by the look of the damaged bucket structures (Fig. 1). In other words, it is conclusive that the FEM model truly simulates the bucket structural behaviour under the action of external loads.

For two years, the average number of the BWE operating hours per year was $T_{year} = 3976$ h. The number of speed of the BW is $n_{BW} = 7.5\ \text{min}^{-1}$, which means that the average number of loading cycles per bucket per year was

$$N_{year} = 60 n_{BW} T_{year} = 60 \times 7.5 \times 3976 = 1789200\ \text{cycles/year}. \tag{13}$$

Having in mind the fact that the bucket loading due to the resistance to excavation is of a pronounced stochastic character, the following can be stated with certainty: (a) there can never be two identical bucket loading cycles; (b) the extreme bucket load cases (on the basis of which its proof of strength is conducted – Subsection 3) which generate stresses close to or higher than the yield stress appear relatively rarely. According to the previous statements, it is conclusive that the bucket fracture is a consequence of long-term fatigue.

Unacceptably high values of the working stresses are primarily the consequence of nonconformity of the buckets to the excavating method and operating conditions, i.e.: (a) poor geometrical shaping and teeth arrangement; (b) bad geometrical shaping of the bucket; (c) inadequate selection of the bucket body material. The shaping of the bucket and teeth and determination of the teeth arrangement should have been conducted on the basis of a kinematic analysis, using a model which includes all of the relevant parameters of the design solution for the BWE working device, as well as the working regime parameters, which act as a foundation for defining the cutting geometry [24,25]. Inexistence of teeth on the knife corners represents a primal defect in shaping of the bucket cutting element, having in mind the fact that the knife corners “do most of the digging” [7]. Finally, the tensile properties of the material used for the manufacturing of the bucket body (S235J2G3 [14]) do not provide the structural integrity of the bucket subjected to the action of extremely high working loads. A common choice for the production of the bucket body is steel quality grade

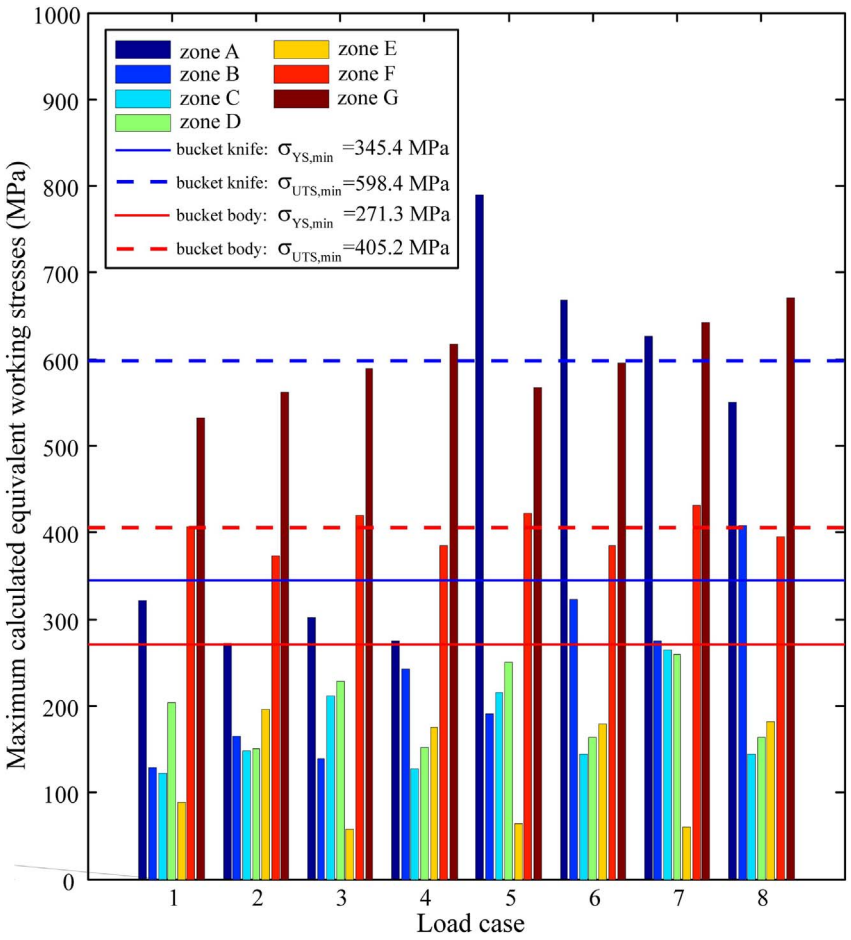

Fig. 13. Equivalent working stress obtained by LFEM for nominal BW drive parameters.

S355J2G3 [14].

5. Conclusion

The results of the numerical-experimental investigation of the working stresses imply that the prime cause for the failure is insufficient strength of the bucket structure. The choice of materials used to produce the bucket body and knives is not in compliance with the recommendations provided by the referent literature [7,9], especially considering their tensile properties. Additionally, the shape of the knife cutting edge, the geometrical form and the arrangement of teeth are not in compliance with the conditions in which the soil cutting process is realised [7–12]. The form of the bucket cutting element (knife and teeth) must be in full compliance with the mining method, i.e. the kinematics of cutting, whereby all of the relevant constructional parameters of the machine, as well as the working regime parameters, must be taken into consideration. This was not the case in the presented study, which is, primarily, confirmed by the fact that there were no teeth installed on the corners of the bucket knife. These facts also provide fertile ground for the occurrence of high values of working stresses. The presented results unambiguously lead to the conclusion that the 'design-in defects' [26] are the dominant cause for the buckets' failure.

High values of residual stresses, as well as the observed cold crack in the welded joint of the knife and the bucket body, point to the significant role of the 'manufacturing-in defects' [26] in the buckets' failure as well.

Finally, the superposition of influences of the 'design-in defects' and 'manufacturing-in defects' has conditioned the appearance and propagation of the long-term fatigue cracks, which led to the total destruction of the buckets.

Acknowledgments

This work is a contribution to the Ministry of Education and Science of Serbia funded project TR 35006.

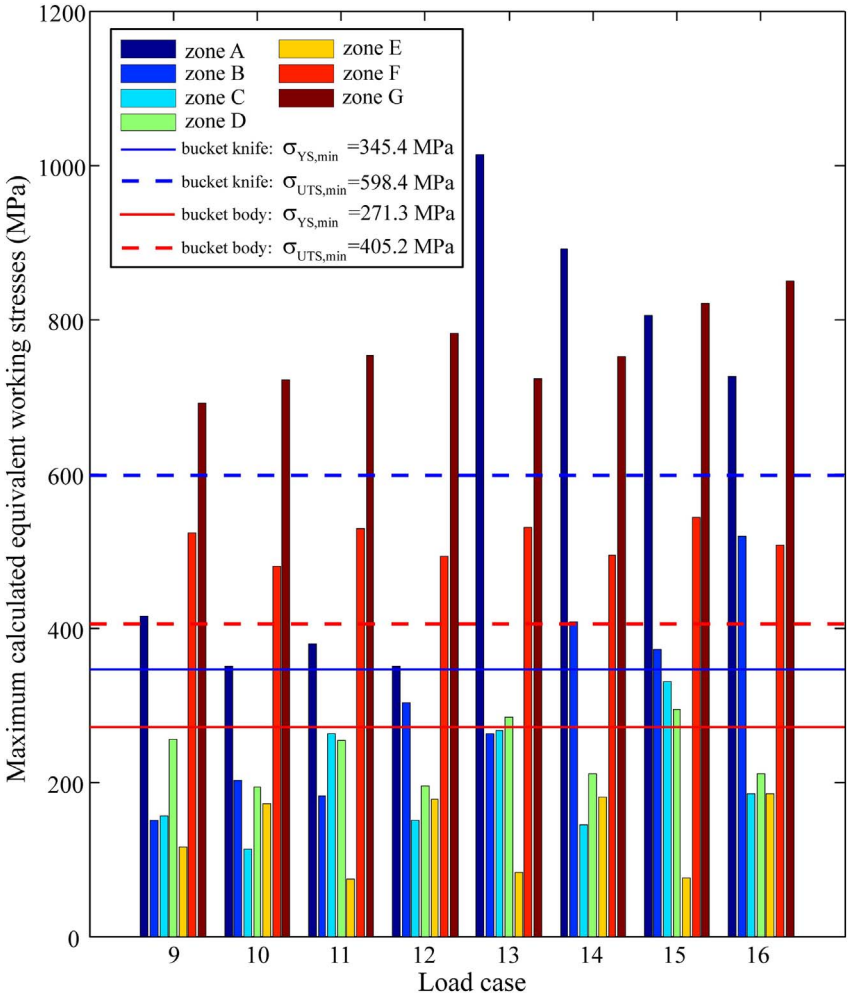

Fig. 14. Equivalent working stress obtained by LFEM for limit BW drive parameters.

References

[1] E. Rusiński, J. Czmochowski, A. Iluk, M. Kowalczyk, An analysis of the causes of a BWE counterweight boom support fracture, Eng. Fail. Anal. 17 (1) (2010) 179–191.
[2] E. Rusiński, P. Harnatkiewicz, M. Kowalczyk, P. Moczko, Examination of the causes of a bucket wheel fracture in a bucket wheel excavator, Eng. Fail. Anal. 17 (6) (2010) 1300–1312.
[3] M. Savković, M. Gašić, M. Arsić, R. Petrović, Analysis of the axle fracture of the bucket wheel excavator, Eng. Fail. Anal. 18 (1) (2011) 433–441.
[4] E. Rusiński, L. Cegiel, A. Michalczyk, P. Moczko, J. Olejarz, D. Pietrusiak, Investigation and modernization of buckets of surface mining machines, Eng. Struct. 90 (2015) 29–37.
[5] T. Smolnicki, G. Pękalski, J. Jakubik, P. Harnatkiewicz, Investigation into wear mechanisms of the bearing raceway used in bucket wheel excavators, Arch. Civ. Mech. Eng. 17 (1) (2017) 1–8.
[6] S. Bošnjak, N. Zrnić, Dynamics, failures, redesigning and environmentally friendly technologies in surface mining systems, Arch. Civ. Mech. Eng. 12 (3) (2012) 348–359.
[7] W. Durst, W. Vogt, Bucket Wheel Excavator, Trans Tech Publications, Clausthal-Zellerfeld, 1989.
[8] D.I. Fedorov, Working Devices of Earthmoving Machines [in Russian], Mashinostroenie, Moscow, 1977.
[9] L. Rasper, Der Schaufelradbagger als Gewinnungsgerat, Trans Tech Publications, Clausthal-Zellerfeld, 1975.
[10] N.G. Dombrovskiy, Multi-bucket Excavators – Constructions, Theory and Calculation [in Russian], Mashinostroenie, Moscow, 1972.
[11] G. Pajer, M. Pfeifer, F. Kurth, Tagebaugroßgeräte und Universalbagger, VEB Verlag Technik, Berlin, 1971.
[12] Yu.A. Vetrov, Soil Cutting by Earthmoving Machines [in Russian], Mashinostroenie, Moscow, 1971.
[13] V.M. Vladimirov, A.I. Shenderov, Mining bucket wheel excavators, Tekhnika, Kiev, 1968 [in Russian].
[14] EN 10025-2, Hot rolled Products of Structural Steels – Part 2: Technical Delivery Conditions for Non-alloy Structural Steels, European Committee for Standardization, 2004.
[15] EN ISO 6892-1, Metallic Materials – Tensile Testing – Part 1: Method of Test at Ambient Temperature, European Committee for Standardization, 2009.
[16] EN ISO 148-1, Mechanical Testing of Metals – Charpy Impact Test – Part 1: Test Method, European Committee for Standardization, 2012.
[17] EN ISO 9016, Destructive Tests on Welds in Metallic Materials – Impact Tests – Test Specimen Location, Notch Orientation and Examination, European Committee for Standardization, 2012.
[18] EN ISO 6506-1, Metallic Materials – Brinell Hardness Test – Part 1: Test Method, (2014).
[19] I. Hrivnák, Theory of Weldability of Metals and Alloys, Elsevier Science, Amsterdam, 1992.
[20] EN ISO 17639, Destructive Tests on Welds in Metallic Materials – Macroscopic and Microscopic Examination of Welds, European Committee for Standardization,

2013.
[21] ISO 3057, Non-destructive Testing – Metallographic Replica Techniques of Surface Examination, International Organization for Standardization, 1998.
[22] K. Hoffmann, An Introduction to Stress Analysis and Transducer Design Using Strain Gauges, HBM, 2012, http://www.kk-group.ru/help/Strain_Gauge_Measurements_Book_2012_01.pdf.
[23] P.J. Withers, Residual stress and its role in failure, Rep. Prog. Phys. 70 (2007) 2211–2264.
[24] S. Bošnjak, Comments on "determination and analysis of the theoretical production of a bucket wheel excavator", Arch. Min. Sci. 60 (1) (2015) 283–301.
[25] S. Bošnjak, Z. Petković, N. Zrnić, G. Simić, A. Simonović, Cracks, repair and reconstruction of bucket wheel excavator slewing platform, Eng. Fail. Anal. 16 (5) (2009) 1631–1642.
[26] C.R. Gagg, Failure of components and products by 'engineered-in' defects: case studies, Eng. Fail. Anal. 12 (6) (2005) 1000–1026.